The end of nanochannels

Thomas B. Sisan[1], *Seth Lichter* *

Abstract: Current theories of nanochannel flow impose no upper bound on flow rates, and predict friction through nanochannels can be vanishingly small. We reassess neglecting channel entry effects in extremely long channels and find violations at the nanoscale. Even in frictionless nanochannels, end effects provide a finite amount of friction. Hence, the speed at which nanochannels transport liquids is limited. Flow-rate and slip length measurements are reevaluated using calculations which include end-effect friction. End effects are critical for the design of new technological devices and to understand biological transport.

Keywords: Nanoscale fluid flow, Nanotubes, Aquaporin

Nanoscale channels, such as aquaporin and carbon nanotubes, exhibit surprisingly large flow rates (Preston et al 1992; Hummer et al 2001; Kalra et al 2003; Falk et al 2010; Thomas and McGaughey 2008). Filtration membranes fabricated from carbon nanotubes have been reported with flow rates 100 - 100,000 times greater than have been measured for any other material (Majumder et al 2005; 2011; Holt et al 2006; Du et al 2011). Arbitrarily high measured flow rates are fit to theoretical calculations by choosing sufficiently small values for the friction parameter along the channel length (Majumder et al 2005; Holt et al 2006; Du et al 2011). These calculations, however, ignore *end effects*, viscous losses within the liquid near the channel's entrance and exit. For nanotubes whose typical lengths are 1000's times their radii, classical fluid dynamics predicts that the great length of the channel provides the primary flow resistance and thus, end effects are negligible. The narrow and tortuous channel of aquaporin leads to similar expectations of negligible end effects. However, contrary to usual fluid mechanics practice and expectation, our results show that long low-friction channels and short channels of any channel friction can have significant end effects. Thus, all treatments of nanochannel flow must be aware of end effects. Friction due to end effects is essential for calculating physically realistic values for flow rates in nanochannels such as carbon nanotubes and aquaporin. Our modified Hagen-Poiseuille equation (see Methods) gives predictions comparable to molecular dynamics results (Kalra et al 2003; Suk and Aluru 2010; Thomas and McGaughey 2009; Goldsmith and Martens 2009). In addition, our results provide a theoretical limit to flow rates in any

[1]Dept of Physics, Northwestern University, Evanston, IL 60208, USA

*Corresponding author, Dept of Mechanical Engineering, Northwestern University, E-mail: s-lichter@northwestern.edu, Phone: 847-467-1885

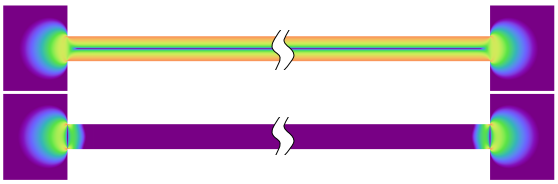

Figure 1. Energy dissipation (high (red), low (purple)), represented by a perceptually balanced color scale (see Methods), as numerically computed for a cylindrical channel between two large reservoirs (2-D cross-section, only a small portion of the reservoirs is shown). For a traditional high-friction "no-slip" channel (top panel), energy dissipation occurs predominantly along the channel length. For a zero-friction channel (bottom panel), energy dissipation occurs solely near the entrance and exit of the channel, irrespective of channel length, in regions of high streamline curvature.

nanochannel, and serve as an upper bound for experimental measurements.

For short aquaporin or slippery carbon nanotube channels, total resistance within the channel can be surprisingly small. Previous efforts to compute flow rates through these channels have focused exclusively on the friction within the channel. But, regions of high viscous shear persist near the channel ends, where streamlines sharply curve from the large reservoirs into (and out of) the small lumen of the channel, see **Figure 1** (Sampson 1891; Weissberg 1962; Suk and Aluru 2010). The size of these localized regions is small, on the order of the channel radius, yet including them in theoretical calculations shows their contribution to flow resistance can be significant. In the limit of zero channel friction $(f = 0)$, flow resistance arises solely through shear in these regions near the channel ends, see Figure 1, bottom panel, thus creating a fundamental flow-rate speed limit, in contrast to prior theory.

Figure 2 shows experimental measurements (symbols) of flow rate in channels of various lengths, L.

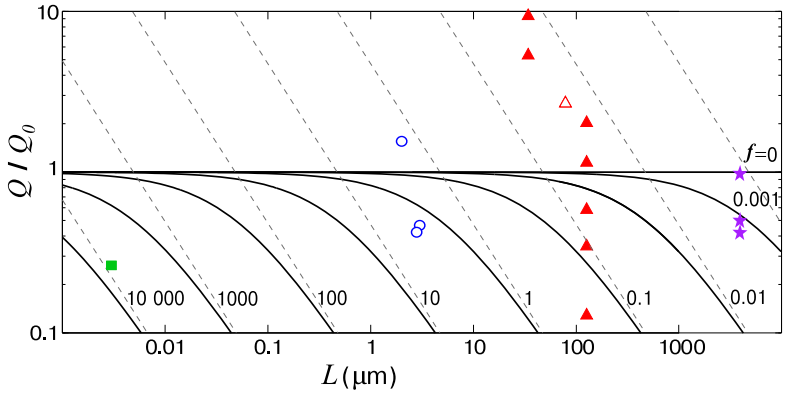

Figure 2. A flow rate speed limit in nanochannels. Predictions (solid lines) of flow rate Q with channel friction f relative to the frictionless-channel flow rate Q_0, versus channel length L, are compared with measurements of carbon nanotubes (blue circles (Holt et al 2006); red triangles, filled (Majumder et al 2005) and open (Majumder et al 2011); purple stars (Du et al 2011)) and aquaporin (green square (Preston et al 1992)). Several reported flow rates (Majumder et al 2005; 2011; Holt et al 2006) are larger than allowed for frictionless channels, $f = 0$. The dashed lines show predictions, for each value of f, when ignoring end effects (Majumder et al 2005; Holt et al 2006; Du et al 2011). These lines erroneously suggest that any Q, no matter how large, is theoretically possible.

Predictions that ignore end effects (dashed lines) increase without bound, so a value of the friction factor f can be found to fit any empirical measurement (Majumder et al 2005; Holt et al 2006; Du et al 2011). Predictions that include end effects (solid lines) asymptote to a maximum flow rate, Q_0. The nine measurements that fall below this line $(f = 0)$ comply with known physics of fluid flow, while the six above this line are unphysically fast. For measurements below the limit, the theory predicts new lower values of f, and thus higher values of the *slip length* (see Methods). For example, new predictions for the two overlapping blue circles, see Figure 2, give values for the friction factor (slip length) that are half (twice) as large as previously found. For flow measurements closer to the limit Q_0, the discrepancy between old and new predictions diverges.

In summary, as friction within channels decreases, end effects make an increasingly large contribution to total flow resistance, see **Figure 3**, even in extremely long channels where end effects have been rotely neglected. For short channels, such as aquaporin, end effects remain significant, asymptoting to a finite value, regardless of the amount of channel friction, see Figure 3, green line. In previous calculations, which omitted end effects, flow rates were unbounded as $f \to 0$. Since viscous losses at the channel entry and exit are independent of channel friction, including them produces an upper limit to the flow rate (Figure 2). Prior measurements that show flow rates above this limit may point to difficulties in accurately determining channel radii, net flow rates, or the number of channels spanning the membrane. Errors may also arise due to compromise in membrane integrity. Appreciation of end losses is necessary for understanding the high, but not unphysically high, flow rates found in carbon nanotubes, so as to ultimately realize the far-reaching

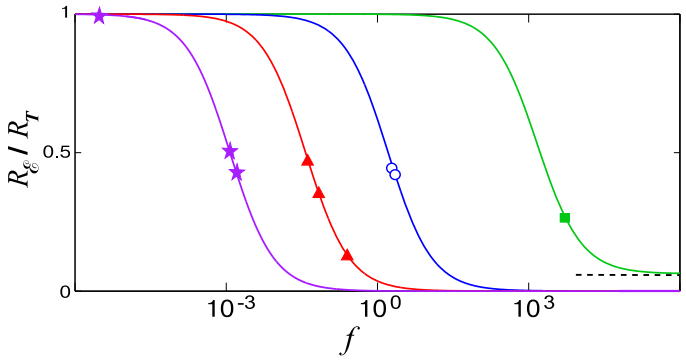

Figure 3. Low friction channels are dominated by end effects. As channel friction f decreases, flow resistance $R_\mathscr{E}$ due to viscous friction at the entrance and exit becomes a larger fraction of the total flow resistance R_T. The colored lines use the channel length, channel radii, pressure drop, and fluid viscosity of the experimental measurements using Equations 2 and 3 (see Methods). The symbols (same as in Figure 2) correspond to those data in Figure 2 below the line $f = 0$, and are placed here by solving Equation 5 (see Methods). Surprisingly, extremely long channels (purple, red, and blue data) can show significant end effects. Limit of green line as $f \to \infty$ is $\sim R/L$ (dashed line).

applications of fluid-transporting nanochannels. Our results also indicate that end effect friction in biological channel entryways may be a significant component in determining and controlling flow rates (Hummer et al 2001).

Discussion: The validity of our continuum scale predictions have yet to be carefully tested for the narrowest channels where molecular discreteness effects may be prominent. The published flow rates from molecular dynamics studies (Kalra et al 2003; Suk and Aluru 2010; Thomas and McGaughey 2008; Goldsmith and Martens 2009) are close to the frictionless channel limit. This is in contrast to experimental reports which show some flow rates significantly above this limit, see Figure 2. However, the molecular dynamics studies do point to areas of further investigation. The pressure drop at the entrance and exit of a channel are predicted by the continuum model to be equal, but in Suk and Aluru (2010), are not. This may indeed be a phenomenon unique to molecular scale flows. However, it may also be a result of the small size of the fluid reservoirs (the continuum model assumes infinite reservoirs), to the unique way in which the upstream and downstream reservoirs are connected, to non steady-state, or even to nonhomogeneous system heating.

Methods: The Hagen-Poiseuille equation gives the pressure drop, neglecting end effects, for fully-developed flow through a cylindrical channel,

$$\Delta P_{HP} = \frac{8\mu LQ}{\pi r^4 + 4\pi r^3/f}, \tag{1}$$

where Q is flow rate, μ is dynamic viscosity, r is channel radius, L is channel length, and the friction factor

$$f = 1/b,$$

where the slip length b quantifies the amount by which the liquid slips along the solid channel wall (Majumder et al 2005; Holt et al 2006). Q diverges to infinity as $f \to 0$.

The pressure drop due to end effects, $\Delta P_{\mathscr{E}}$, is well approximated by the expression for flow through an

aperture (Sampson 1891; Weissberg 1962; Suk and Aluru 2010),

$$\Delta P_{\mathscr{E}} \approx \frac{3Q\mu}{r^3}. \tag{2}$$

Using the expression for total pressure drop across a channel between two reservoirs, $\Delta P_T = \Delta P_{\mathscr{E}} + \Delta P_{HP}$, Equations 1 and 2 give a modified Hagen-Poiseuille equation,

$$\Delta P_T = \left[\frac{3\mu}{r^3} + \frac{8\mu L}{\pi r^4 + 4\pi r^3 b}\right] Q_T \tag{3}$$

where the term in brackets $[\ldots]$ is defined as the total flow resistance R_T, see Figure 3. Equation 3 can be rearranged to give the flow rate in the limit of large slip $(b \gg r)$,

$$Q = Q_0 \left[1 + \frac{2}{3\pi}\frac{L}{b}\right]^{-1}, \tag{4}$$

where $Q_0 = \Delta P_T r^3/3\mu$ is the flow rate through a frictionless channel $(b \to \infty)$, and the subscript T on the flow rate has been dropped for simplicity. Equation 4 takes into account both high slip and end effects in nanoscale channels, in contrast to the normal HP equation (1). By equating the flow rate without and with end effects (Eqs. 1 and 3), the slip length can be expressed in terms of previously-found slip lengths $\cancel{b}$ which neglected end effects, $b = \cancel{b}\,(1 - \frac{3\pi\cancel{b}}{2L})^{-1}$. Experimental measurements which found $\cancel{b}\,/L > 2/3\pi$ are unphysical.

Fabricated carbon nanotube membranes (Majumder et al 2005; Holt et al 2006; Hinds et al 2004; Du et al 2011) are comprised of a heterogenous distribution of nanotube radii, so the total membrane flow rate is

$$Q_M = \sum_{i=1}^{N} Q\left(r_i\right),$$

where N is the number of open nanotubes spanning the membrane and $Q(r_i)$ is the flow rate through channel i. We generate a normal distribution of radii, r_M, based on published radii histograms (Holt et al 2006; Hinds et al 2004; Du et al 2011). From this distribution the flow rate through a membrane comprised of frictionless carbon nanotubes is

	liquid	μ (cp)	N	L (μm)	Q_M (cm^3/s)	r_M (nm)	$Q_{M,0}$ (cm^3/s)	$\mathscr{Q}$	b (μm)
Majumder (2005) et al.	water	1	10^9	34	9.62	$\langle r_M\rangle$=3.5 σ_M=1	1.79	5.37	-
					16.9			9.44	-
			$3.4{\cdot}10^9$	126	12.4		6.07	2.04	-
	ethanol	1.1			5.89		5.06	1.16	-
	isopropanol	2			1.47		3.10	0.47	24.11
	hexane	0.3			7.33		20.7	0.35	14.66
	decane	0.9			0.877		6.75	0.13	3.99
Majumder (2011) et al.	water	1	$2.4{\cdot}10^6$	81	$2{\cdot}10^{-8}$	$\langle r_M\rangle$=3.5 σ_M=1.0	$8.3{\cdot}10^{-9}$	2.40	-
Holt et al.	water	1	$2.5{\cdot}10^{11}$	2	7.47	$\langle r_M\rangle$=0.8 σ_M=0.15	4.68	1.60	-
				3	2.23			0.48	0.58
				2.8	1.97			0.42	0.43
Du et al.	water	1	$2.4{\cdot}10^{10}$	$4{\cdot}10^3$	0.058	$\langle r_M\rangle$=5.0 σ_M=1.0	0.112	0.52	910
	hexane	0.31			0.154		0.362	0.43	630
	dodecane	1.34			0.082		0.084	0.97	30000

Table 1. Data from prior work (Majumder et al 2005; 2011; Holt et al 2006; Du et al 2011) (left of vertical dividing line) and derived values (right of dividing line) used in Figure 1. μ is dynamic viscosity, N number of open nanotubes spanning $1\,\mathrm{cm}^2$ of membrane, L nanotube length, and Q_M total flow rate through $1\,\mathrm{cm}^2$ membrane. For Majumder et al (2005; 2011), Q_M was computed from their published velocities. For Holt et al (2006), Q_M was computed from their published slip lengths. Published distributions of nanotube radii (Holt et al 2006; Hinds et al 2004; Du et al 2011) were used to generate the normal distribution of radii used in the membranes, r_M, with mean $\langle r_M\rangle$ and standard deviation σ_M, used in our calculations. $Q_{M,0}$ is the total flow rate through a $1\,\mathrm{cm}^2$ membrane comprised of frictionless nanotubes of radial distribution r_M. b is the slip length from Eq. 5. Values of $\mathscr{Q} = Q_M/Q_{M,0} > 1$ do not comply with known physics of fluid flow.

$$Q_{M,0} = \sum_{i=1}^{N} Q_0\left(r_i\right).$$

The slip length can then be determined from Eq. 4,

$$b = L\frac{2}{3\pi}\frac{\mathscr{Q}}{1-\mathscr{Q}}, \tag{5}$$

where $\mathscr{Q} = Q_M/Q_{M,0}$ is the ratio of the measured flow rate to the maximum rate that would occur through the same distribution of frictionless nanotubes.

For aquaporin, data is derived from published osmotic permeabilities p_f (Preston et al 1992) expressed in terms of hydrostatic pressure drop across the channel,

$$\Delta P_T = \frac{\rho kT}{mp_f}Q,$$

where ρ is fluid density, kT is the thermal energy, and m is the molecular mass. The end-effect pressure drop is given by Eq. 2, with the channel radius chosen as the average radius through the single-file portion of the channel.

Values used to produce Figures 2 and 3 and a summary of experimental measurements are given in

Table 1. In the figures, the friction factor, f, is given in units of μm^{-1}. The flow resistance, $R_\alpha = \Delta P_\alpha / Q$, where $\alpha = T, \mathscr{E}$ for total membrane or end-effects, respectively, and ΔP_α is the pressure drop.

In Figure 1, the rate of energy dissipation was calculated from a numerical simulation of the Navier-Stokes equations using an axially symmetric geometry of a cylindrical channel between two large reservoirs with a flow rate of $10^3 \mu\text{m}^3/\text{s}$. A perceptually-balanced color scale in MATLAB was chosen for visual accuracy to reduce luminance variation artifacts of the standard rainbow colormap. In the simulations, changing from slip to no-slip boundary conditions on the reservoir walls had negligible effects on flow rates. Additionally, interactions between neighboring channel openings were investigated by adding a second nearby channel. At the separation for adjacent double-walled carbon nanotubes and internal channel radius 1 nm, such as may occur in fabricated membranes (Holt et al 2006), no significant interactions were observed, in agreement with theoretical predictions (Wang 1994).

Acknowledgements Mark Johnson provided insight into flows through biological pores. Mitra Hartmann and Alphonso Mondragon provided editorial assistance. This work was funded by a generous grant from the A. K. Barlow Foundation.

References

Du F, Qu L, Xia Z, Feng L, Dai L (2011) Membranes of vertically aligned superlong carbon nanotubes. Langmuir 27:8437–8443, DOI 10.1021/la200995r

Falk K, Sedlmeier F, Joly L, Netz RR, Bocquet L (2010) Molecular origin of fast water transport in carbon nanotube membranes: Superlubricity versus curvature dependent friction. Nano Lett 10(10):4067–4073, DOI 10.1021/nl1021046

Goldsmith J, Martens CC (2009) Pressure-induced water flow through model nanopores. Phys Chem Chem Phys 11:528–533, DOI 10.1039/B807823H

Hinds BJ, Chopra N, Rantell T, Andrews R, Gavalas V, Bachas LG (2004) Aligned multiwalled carbon nanotube membranes. Science 303(5654):62–65, DOI 10.1126/science.1092048

Holt JK, Park HG, Wang Y, Stadermann M, Artyukhin AB, Grigoropoulos CP, Noy A, Bakajin O (2006) Fast mass transport through sub-2-nanometer carbon nanotubes. Science 312(5776):1034–1037, DOI 10.1126/science.1126298

Hummer G, Rasaiah JC, Noworyta JP (2001) Water conduction through the hydrophobic channel of a carbon nanotube. Nature 414(6860):188–190, DOI 10.1038/35102535

Kalra A, Garde S, Hummer G (2003) Osmotic water transport through carbon nanotube membranes. Proc Natl Acad Sci USA 100(18):10,175–10,180, DOI 10.1073/pnas.1633354100

Majumder M, Chopra N, Andrews R, Hinds BJ (2005) Nanoscale hydrodynamics: Enhanced flow in carbon nanotubes. Nature 438(7064):44, DOI 10.1038/43844a

Majumder M, Chopra N, Hinds BJ (2011) Mass transport through carbon nanotube membranes in three different regimes: Ionic diffusion and gas and liquid flow. ACS Nano DOI 10.1021/nn200222g

Preston GM, Carroll TP, Guggino WB, Agre P (1992) Appearance of water channels in Xenopus oocytes expressing red cell chip28 protein. Science 256:385–387, DOI 10.1126/science.256.5055.385

Sampson RA (1891) On Stokes's current function. Phil Trans R Soc Lond A 182:449–518, DOI 10.1098/rsta.1891.0012

Suk ME, Aluru NR (2010) Water transport through ultrathin graphene. J Phys Chem Lett 1(10):1590–1594, DOI 10.1021/jz100240r

Thomas JA, McGaughey AJH (2008) Reassessing fast water transport through carbon nanotubes. Nano Lett 8(9):2788–2793, DOI 10.1021/nl8013617

Thomas JA, McGaughey AJH (2009) Water flow in carbon nanotubes: Transition to subcontinuum transport. Phys Rev Lett 102(18):184,502, DOI 10.1103/PhysRevLett.102.184502

Wang CY (1994) Stokes flow through a thin screen with patterned holes. AIChE J 40(3):419–423, DOI 10.1002/aic.690400305

Weissberg HL (1962) End correction for slow viscous flow through long tubes. Phys Fluids 5(9):1033, DOI 10.1063/1.1724469